PAPER NUMBER

17

CORROSION 85

The International Corrosion Forum Devoted Exclusively to The Protection and Performance of Materials

March 25-29, 1985 / Sheraton Hotel
Hynes Auditorium / Boston, Massachusetts

FIELD EXPERIENCE WITH ENGINEERING MATERIALS IN INDUSTRIAL HEAT RECOVERY SYSTEMS

M. F. Rothman
Cabot Corporation
1020 West Park Avenue
Kokomo, Indiana 46901

G. Y. Lai
Cabot Corporation
1020 West Park Avenue
Kokomo, Indiaa 46901

D. E. Fluck
Cabot Corporation
1020 West Park Avenue
Kokomo, Indiana 46901

ABSTRACT

Results of field exposures of multiple alloy coupon racks, failure analyses of actual components and related laboratory evaluations of different alloys are all discussed in an effort to describe the nature of materials behavior in various high-temperature industrial recuperator environments. Environments evaluated included those in molten fiberglass production facilities, primary and secondary aluminum remelting facilities, and a zinc melting furnace. Wide variation in materials performance was observed as a consequence of the many forms of high-temperature corrosion encountered. Included in these were oxidation/sulfidation, oxidation, alkali-halide fluxing, sulfate fluxing, and chlorination/oxidation among others. Corrosion rates measured in various rack and component tests ranged from less than 50 mpy (1.3 mm/year) to over 700 mpy (17.8 mm/year) for the best performing materials. By means of the examples cited, it is demonstrated that the nature of the high temperature corrosion problems in heat recovery systems dictates that careful consideration must be given to selecting the best materials of construction on a case by case basis.

INTRODUCTION

One of the important trends emerging from the push for improved energy efficiency in many industries is the growing use of waste heat recuperation from high-temperature process gas streams and waste gases. This approach has been quite

successful in producing significant reductions in fuel costs for a number of specific "clean" industrial applications, and the economics of waste heat recupertion have been treated in some detail by several authors[1-5]. These types of analyses usually address the question of the reduction in fuel costs to be achieved as a function of increasing the combustion air preheat temperature with heat recuperated from flue gases. Little or no mention is normally made of the recuperator material or the need for it to resist the environment. This is perhaps indicative of the general unimportance of high-temperature corrosion problems in the "clean" flue gas systems being considered.

Within recent years, the application of waste heat recuperation technology has spread to industrial processes with far more corrosive high-temperature flue gas environments. Some of these include the primary metals industry (aluminum, zinc, copper, lead), the glass industry, and general industrial heating applications employing low-grade or contaminated fuels. The specific nature of these corrosive high temperature environments and the capabilities of various engineering materials to cope with them in recuperator applications are not well known. Systematic evaluations of materials performance in individual industrial waste heat recuperator environments such as these have been limited, and little data are available which describe the mode of failures experienced by materials in actual component applications.

The intent of this paper is to develop an appreciation of the performance characteristics of various engineering materials which could be employed in the application of waste heat recovery technology to several of these industrial processes. Results of field testing of multiple alloy coupon test racks and of failure analyses performed for actual components will be presented. Examples of material's behavior will be discussed for waste heat recuperators in the glass industry, the aluminum melting industry and the zinc melting industry. Nominal compositions of alloys discussed in this paper are given in Table 1.

GLASS MELTING

Multiple alloy coupon rack exposures were performed in the recuperator of a fiberglass melting furnace. The double shell, radiant-type recuperator made from alloy 601 had been experiencing severe localized pitting attack in the area corresponding to metal temperatures of 1200°F (650°C). Two different exposures were performed for melting campaigns involving the different glass formulations normally melted in that furnace. Racks were positioned in the flue gas stream at a location corresponding to a flue gas temperature of 1200°F (650°C). Rack No. 1 was exposed for about 500 hours, and Rack No. 2 was exposed for about 850 hours. Pictures of the as-exposed racks are shown in Figure 1.

It is obvious from the appearance of the racks that they were exposed to different conditions. Rack No. 1 had crusty deposits which were apparently solid at the exposure temperature, while the deposits on Rack No. 2 were clearly liquid, as evidenced by the frozen droplets at the bottom corners of some of the coupons. This factor, in addition to the variation in glass composition, could certainly be expected to produce a difference in specific alloy corrosion behavior.

Results of the evaluation of alloy corrosion behavior obtained from the two test racks are presented in Figures 2 and 3. In the case of Rack No. 1, the typical attack observed involved oxidation combined with mild sulfidation. From an examination of Figure 2, it is evident that the high nickel and low chromium materials such as alloy S (67% Ni, 16% Cr) and alloy 600 (74% Ni, 16% Cr) were most severely attacked. The higher iron and chromium materials like alloy 601 (61% Ni, 14% Fe, 22% Cr) and alloy 800H (33% Ni, 44% Fe, 21% Cr) fared only a little better. The materials most resistant to uniform corrosion

were alloy X (47% Ni, 19% Fe, 22% Cr) and 310 stainless steel (20% Ni, 51% Fe, 25% Cr), although the 310 stainless did exhibit appreciable localized pitting.

The poor behavior of the high nickel and high nickel plus iron alloys would be expected under a corrosion mode dominated by high-temperature sulfidation. This is consistent with the laboratory studies performed by Lai[6]. The superior performance of alloy X with its high nickel plus iron content is unexplained in this case, however, since its resistance to sulfidation as determined by Lai is no better than that of the alloys previously mentioned, including alloy 601. Nevertheless, the role of subsurface sulfide formation in the corrosion of the high nickel alloys like alloy 601 has been confirmed metallographically, as shown in Figure 4. It would appear that chromium depletion through sulfide formation followed by accelerated oxidation of the chromium depleted areas is a likely partial appreciation of the corrosion mechanism, but other factors such as the role of highly reactive glass vapor components containing K and Ca must surely be involved. This is supported by the SEM micrograph and associated EDAX analyses presented in Figure 5 for a sample of the cobalt-base alloy 25 chain used to support a test rack, albeit in a hotter part of the recuperator. Clearly, K and Ca are major constituents in the corrosion products.

The alloy ranking for the second test rack exposed in the fiberglass melting furnace recuperator differs significantly from that obtained in the first rack exposure. As shown in Figure 3, the alloys most resistant to uniform corrosion were three of the four worst performing alloys in the first test, including alloy 601. Although this is consistent with the fact that there was no evidence of sulfidation, the more important factor is the change in the nature of the deposits from solid to liquid phase. The mode of corrosion here most likely involves molten glass fluxing of protective oxide scales with subsequent internal oxidation attack. These are similar in nature to the conditions which molten glass holding pots and fiberglass drawing pots must withstand. Materials such as alloy 600 are normally employed with success in these applications.

Although alloy X falls in the middle group of materials in terms of these second test rack results, it is important to note that it exhibits uniform thinning. Several of the materials more resistant to uniform corrosion, including alloy 601, exhibit appreciable localized pitting. This is illustrated in Figure 6. In terms of minimum remaining unaffected metal, these alloys would rank worse than alloy X, though certainly still better than the least-resistant materials.

ALUMINUM MELTING

Several failure analyses and multiple alloy coupon rack exposures were performed relative to materials problems in tubular-type recuperators in aluminum melting furnace facilities. These facilities included reverberatory scrap melting furnaces in which halide fluxes are used to remove oxides on the bath surface and hydrogen purging is often achieved through bubbling chlorine-containing gases through the melt. Multiple alloy coupon exposures were also performed in the recuperator of a remelting furnace in a die casting plant, where only chlorine gas purging was employed.

A typical failure analysis was performed for a corroded tube of 12% Cr ferritic stainless exposed for about 6 months in the recuperator of a scrap aluminum remelt furnace. The recuperator was operating in up to about 1800°F (980°C) flue gas, but yielding only 750°F (400°C) preheated air, so O.D. surface metal temperatures were probably only somewhere between about 1000°F to 1400°F (540°C to 760°C). Typical NaCl-KCl-Cryolite-type fluxes were used, which were claimed to be low in sulfur. Charge materials included old beer cans and kegs with lacquer and printing on the surface. The tubes in this recuperator

perforate every 6 months as a consequence of corrosion, and exhibit a greenish-yellow scale.

A piece of the failed tubing was sectioned and subjected to SEM EDAX semi-quantitative analysis. Typical SEM through-thickness photomicrographs and related EDAX analyses are presented in Figures 7 and 8. From an examination of Figure 7 it is clear that, despite the use of sulfur-free fluxes, sulfur is present in the surface scale as is chlorine, calcium and potassium. Small amounts of sodium, lead and even bromine were also found in other spots. The calcium- and silicon-rich particle on the surface may be from the melting furnace refractory. The other scale areas are probably mixtures of compounds such as Fe_2O_3, $FeCl_2$, KCl and K_2SO_4. The low chromium content in these scales is consistent with the concept of surface chromium depletion by alkali-halide fluxing of chromium-bearing protective oxide scales (possibly combined with sulfidation) advanced by Russell et al.[7], and also with the possible formation of volatile chromium oxychloride compounds proposed by Saunders and Schlierer[8].

The SEM photomicrograph shown in Figure 8 reveals that general corrosion is not the only form of material degradation being experienced by the tubes of 12% Cr ferritic stainless. Internal cracks were observed which had apparently initiated at the site of glassy-looking particles on the tube surface. These particles appear once again to be basically iron-chloride/oxide mixtures with sulfur and potassium also present.

Multiple alloy coupon rack exposures are being pursued at this particular facility, but such tests have alrady been performed in another scrap melting furnace recuperator. Metal temperatures in these tests were considerably higher than those in the case of the failure analysis just discussed, however. The un-cooled coupons were exposed to 1650°F to 1800°F (900°C to 980°C) flue gases in a reverberatory aluminum melting furnace recuperator for only 120 hours. Operating procedures for this facility involved the use of the same NaCl-KCl-Cryolite-type fluxes previously mentioned. Again, these fluxes were reputed to be "sulfur-free."

Figure 9 shows the ranking of material performance in these tests for 12 commercial alloys, and some typical through-thickness microstructures are presented in Figure 10. Despite the short duration of the exposure, the extreme aggressiveness of the environment is evidenced by the substantial amount of metal wastage and internal penetration experienced by even the best performing material, alloy 556. This severe amount of material degradation had not been expected in view of other experiences with similar "sulfur-free" environments.

Suspecting that the environment might contain sulfur or other contaminants despite the claims of the flux suppliers, chemical analyses for the different flux components was performed. It was determined that the various flux components did, in fact, contain up to as much as 2.1% sulfur. Such contamination would serve to explain the results illustrated in Figure 11, in which an SEM photograph of the scale formed upon the 304 stainless steel coupon is shown together with EDAX analyses of various areas. The presence of a heavy concentration of sulfur at the scale/metal interface is clearly revealed.

It is notable that, unlike the case of the failure analysis previously discussed, no potassium-, sodium- or chlorine-rich areas were observed for any of the coupons exposed in these tests. As the temperature of exposure was in excess of 1650°F (900°C), this might well be anticipated since the NaCl and KCl constituents present in the flue gases as a result of vaporization of the added fluxes would not be expected to condense at these temperatures. It is certainly possible that Na_2SO_4 and K_2SO_4 reaction products form at 1650°F (900°C); however, excursions to 1800°F (980°C) would tend to inhibit such sulfate deposition on the sample surfaces. It seems most likely

that the mode of corrosion taking place in this higher-temperature regime is a combination of gas/metal sulfidation and gas/metal chlorination-oxidation.

The reasons for the ranking of material performance presented in Figure 9, albeit from bad to worse, are not immediately obvious. There appears to be little similarity among those materials which exhibit the most resistance and, for that matter, among those which exhibit the least resistance. The aluminum-oxide-forming alloy 214 appears to behave little different from the chromia-forming alloys. Iron-base, nickel-base and cobalt-base alloys exhibit no particular distinctiveness. High refractory element content alloys such as alloy 188 and alloy S exhibit perhaps an increased amount of metal loss, but no more than 304 stainless steel, which has no refractory element content. HASTELLOY alloy X, by the same token, has 9% molybdenum and exhibits the least metal loss of the alloys tested.

The only potentially important factor which singles out alloy 556 from the other alloys is the fact that, in laboratory test results reported by Lai[6] for sulfidation and McNallan et al.[9] for exposure in Ar-20% O_2 - 0.25% Cl_2 environments, alloy 556 was the only alloy in the present tests which performed well in both studies. Alloy 625 exhibited reasonably good sulfidation resistance at 1600°F (870°C) in Lai's study, but was undistinguished in the 1650°F (900°C) chlorination-oxidation study performed by McNallan et al.

It is clear that the temperature of the flue gases is a critical consideration in terms of the mode of high-temperature corrosion to be expected. This is illustrated to some degree by the results of another multiple coupon rack exposure performed in the recuperator of an aluminum melting furnace at a die casting plant. In this operation no fluxing agents were employed, although purging of hydrogen from the molten metal was achieved by bubbling chlorine-containing gases through the melt. The test rack was exposed to 1400°F to 1500°F (760°C to 815°C) flue gases for about six weeks.

Results of this test exposure are given in Figure 12 for twelve commercial materials, and typical through-thickness photomicrographs for several materials are presented in Figure 13. It is immediately clear that the rates of corrosion observed in this case are as much as an order of magnitude lower than those in the previous case. This is likely a function both of the lower temperature and, perhaps even more importantly, of the absence of potassium-, sodium- and sulfur-containing compounds, excluded as a consequence of not employing fluxing agents.

The best performing material in these tests was alloy 188, a cobalt-base alloy. The next best materials were all nickel-base, including the high-aluminum alloy 214. None of these materials suffered large wastage of metal, but rather the bulk of the degradation observed was in the form of internal penetration. As may be seen in Figure 13, this internal penetration was in many cases along grain boundaries. Sometimes, as in the case of alloy 601, this grain boundary attack was accompanied by severe intragranular void formation. This is believed to be associated with the secondary attack of matrix carbides which precipitate after carbon freed from chlorinated grain boundary carbides has diffused out into the matrix. Such behavior has been observed in laboratory tests conducted by Elliott et al.[10] for materials such as alloy 800H in air plus 2% Cl_2 environments at 1000°C (1832°F).

The superior performance of alloy 188 in these 1400°F to 1500°F (760°C to 815°C) exposures is in marked contrast to the 1650°F (900°C) laboratory test results in Ar-20% O_2 - 0.25% Cl_2 reported by McNallan et al.[9], which found alloy 188 last in performance among those alloys tested (many of which trailed alloy 188 in performance in these field exposures). McNallan has proposed that the particularly poor performance of alloy 188, among

others, is attributable to the formation of volatile refractory metal oxychlorides. Such a reaction would be accelerated by rapid ingress of oxygen and chlorine resulting from breakdown of chromia scale protection on these alloys by formation of liquid chromium chlorides which melt at about 1510°F (820°C). These liquid chromium chlorides would likely be rapidly oxidized to form volatile chromium oxychlorides at these temperatures.

By the same token, at exposure temperatures less than the melting point of chromium chloride, such as is the case with the present field test, the kinetics of chromium oxychloride formation would be much slower as a consequence of the slower diffusion rates of both oxygen and chlorine through the solid chloride/oxide scale. This could serve to explain the better performance of all of the chromia forming alloys, particularly as regards the low rate of metal wastage.

As for internal attack, all of the alloys which were at the top of the list in terms of performance, with the exception of alloy 214, contain sufficient amounts of molybdenum, tungsten, columbium, tantalum or titanium to have primary carbides which are low in chromium content (M_6C, MC) rather than chromium-rich carbides ($M_{23}C_6$, M_7C_3). Such carbides should not be as readily chlorinated as the chromium-rich carbides. Neither would they be associated with chromium depletion in the surrounding matrix. Both of these factors could contribute to the observed higher level of resistance in the field exposure as compared to the higher-temperature laboratory tests. For the alloys which form principally chromium-rich carbides, the slowed rate of chlorine and oxygen ingress would yield less overall internal penetration, but these carbides and surrounding chromium-depleted areas would be more heavily attacked. Typical massive internal chromium chloride formation and associated chromium depleted metal areas are shown for 310 stainless steel in the SEM photomicrograph and EDAX analyses of Figure 14.

ZINC MELTING

A failure analysis was performed for tubes of type 316 stainless steel exposed in the recuperator of a zinc melting furnace. A silicon carbide crucible placed in a combustion chamber and heated by combustion of natural gas was used to melt and vaporize zinc. Supposedly isolated from the molten/vapor zinc environment, the combustion flue gases were passed through the recuperator to preheat combustion air. The flue gas temperature was reported to be 1800°F (980°C), while preheat combustion air temperature was given as 1000°F (540°C), leaving actual tube metal temperatures somewhere in between. All of the Type 316 stainless steel tubes examined from the recuperator front row failed after only two to three months service due to severe corrosion attack. A section of a corroded tube from the first row in the recuperator is shown in Figure 15.

Metallographic examinations were performed for the failed tube from the front row of the recuperator and a tube from the third row of the recuperator. Samples were taken at locations facing the direction of flue gas flow. Typical through-thickness microstructures are shown in Figures 16 and 17, respectively. The perforated tube from the front row exhibited clear signs of localized catastrophic oxidation, while the tube in the third row was far less severely attacked. The scale, in both cases, was found to be essentially iron-chromium-rich presumably spinel-type oxide containing substantial amounts of zinc contamination, all confirmed by SEM/EDAX analysis. Some small amount of sub-scale sulfide formation was also noted.

Apparently, zinc leakage through the crucible into the combustion chamber reacted with oxygen in the flue gas to form zinc-rich oxides on the tube surfaces. This resulted in localized accelerated oxidation attack and the eventual perforation of the tubes in the front row of the recuperator. The better performance

of the tubes in the third row may be due to both the effects of lower temperature, since the flue gases would be cooler at this point, and the depletion of zinc or zinc oxide from the flue gas stream by the deposition/reaction with the tubes in the first two rows.

Figure 18 is a through-thickness photomicrograph of the microstructure of a 309 stainless steel baffle plate located between the third and fourth row of tubes. This plate, which was uncooled, probably experienced flue gas temperatures close to those of the front row of tubes. Since the degree of attack exhibited by the plate is not much more than that of the cooled tube in the third row, it would appear that zinc vapor or zinc oxide content in the flue gas may be a more over riding consideration than temperature in this case. Of course, the difference between the performance of Type 309 versus Type 316 stainless steel clouds the issue to some extent.

At any rate, the key factor involved in the degradation of the tubes in the recuperator of this zinc melting facility was the presence of zinc vapor or oxide in the flue gas stream. The presence of sulfur derived from the natural gas as a minor contaminant or perhaps from elsewhere in the system was also a contributing factor.

SUMMARY & CONCLUSIONS

A variety of field experiences with recuperator materials of construction have been presented for flue gas environments which pose severe high-temperature corrosion problems. Among the cases considered were recuperators in glass melting, aluminum melting and zinc melting facilities. It is clear from these examples that the varying nature of the high-temperature corrosion problems to be expected dictates careful consideration of the most suitable materials of construction on a case by case basis. In the particular instances of aluminum melting facilities, widely different rankings of materials performance were observed as a function of operating conditions. In glass melting, two different glass compositions yielded significantly differing modes of corrosion and correspondingly different alloy performance rankings.

Among the types of high-temperature corrosion phenomena encountered in these various waste heat recovery applications were oxidation/sulfidation, oxidation, alkali-halide fluxing, sulfate fluxing, chlorination/oxidation, and zinc vapor-oxide accelerated oxidation. In addition to these, it would not be inappropriate to also include potential molten glass fluxing, molten zinc fluxing and corrosion involving aluminum in both the vapor and liquid phases, though none of these were directly observed. In view of the diversity of hostile, corrosive conditions to be dealt with, it is also possible that these modes of corrosion could be encountered in combination. Despite this somewhat gloomy situation it is clear that, in some cases, rational choices from among existing commerical alloys can be made for obtaining acceptable levels of performance. In other cases, the situations represent challenging opportunities for alloy development.

REFERENCES

1. J. Seehausen, Industrial Heating, Vol. LI, No. 1, p. 25 (1984).

2. J. L. Ferri and K. H Kohnken, Heat Treating, Vol. XV, No. 9, p. 35 (1983).

3. D. A. Zurawski, Industrial Heating, Vol. XLVIII, No. 6, p. 8 (1981).

4. J. Seehausen, "Reliability, Efficiency and Economics of Recuperators in Industrial Applications," presented at the International Gas Research Conference, Los Angeles (1981).

5. N. L. Moore, "State of-the-Art of Furnace Recuperation in the Primary Metals Industry: Technical Briefing Report," Battelle Pacific Northwest

Laboratory Report, PNL-4803, August 1983.

6. G. Y. Lai, Paper No. 73, presented at Corrosion/84, NACE, New Orleans, Louisianna, April 1984.

7. A. D. Russell, C. E. Smeltzer, and M. E. Ward, "Waste Heat Recuperation for Aluminum Furnaces", Gas Research Institute Report, GRI 5081-342-0493, April 1983.

8. S. J. Saunders and S. Schlierer, "Sulfidation of Coal Gasifier Heat Exchanger Alloys," presented at "High Temperature Corrosion in Energy Systems," Detroit, Michigan, September 1984.

9. M. J. McNallan, M. H. Rhee and M. F. Rothman, "Long Term High-Temperature Corrosion Studies of High Temperature Alloys in Chlorine-Contaminated Environments," presented at "High Temperature Corrosion in Energy Systems," Detroit, Michigan, September 1984.

10. P. E. Elliott, A. I. Ansari, M. F. Rothman, Paper No. 13, presented at Corrosion/85, NACE, Boston, Massachusetts, March 1985.

Table 1
ALLOYS INCLUDED IN STUDIES

Material	Nominal Composition (Wt. %) Ni	Fe	Co	Cr	Mo	W	Al	Ti	C	Others
HASTELLOY® alloy X	BAL	19	1.5	22	9	0.6	-	-	.10	
HASTELLOY alloy S	BAL	3*	-	16	15	-	-	-	.02*	.009 B, 0.5 Si, .02 La
Alloy 625	BAL	5*	-	21	9		0.4*	0.4*	.04	3.5 Cb
CABOT® alloy No. 214	BAL	4	-	16	-	-	4.2	-	.05	.01 Y
WASPALOY alloy	BAL	2*	14.0	19	4	-	1.5	3.0	.05	.05 Zr, .006 B
Alloy 600	BAL	8	-	16	-	-	-	-	.04	
INCONEL® alloy No. 601	BAL	14	-	23	-	-	1.4	0.3	.10*	
Type 304 Stainless	9	BAL	-	18	-	-	-	-	.05	
Type 309 Stainless	14	BAL	-	22	-	-	-	-	.15	
Type 310 Stainless	19	BAL	-	25	-	-	-	-	.10	
Type 316 Stainless	12	BAL	-	17	2	-	-	-	.06	
Alloy 330	35	BAL	-	19	-	-	-	-	.05	1.3 Si
Alloy 800H	33	BAL	-	21	-	-	0.4	0.4	.08	
HAYNES® alloy No. 556	20	BAL	18.0	22	3	2.5	0.2	-	.10	.8 Ta, .2 N, .02 La
HAYNES alloy No. 25	10	3*	BAL	20	-	15.0	-	-	.10	
HAYNES alloy No. 188	22	3*	BAL	22	-	14.0	-	-	.10	.04 La, 0.4 Si

* Maximum

® HASTELLOY, HAYNES and CABOT are trademarks of Cabot Corporation
INCONEL is a trademark of the Inco Family of Companies
WASPALOY is a trademark of United Technologies Co.

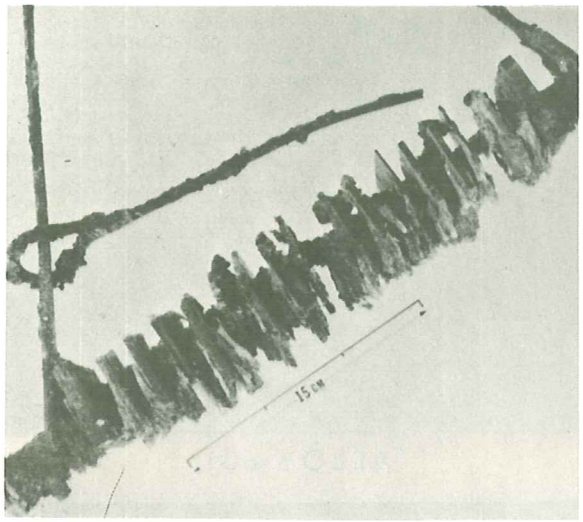

RACK NO. 1

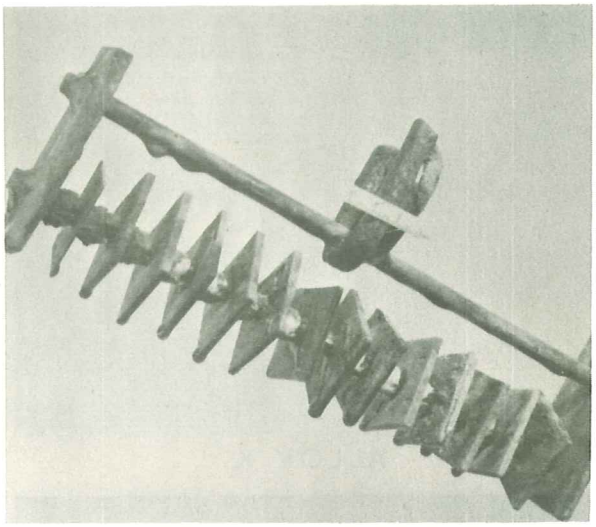

RACK NO. 2

FIGURE 1: APPEARANCE OF TEST RACKS EXPOSED IN A FIBERGLASS MELTING FURNACE RECUPERATOR WITH TWO DIFFERENT GLASS FORMULATIONS.

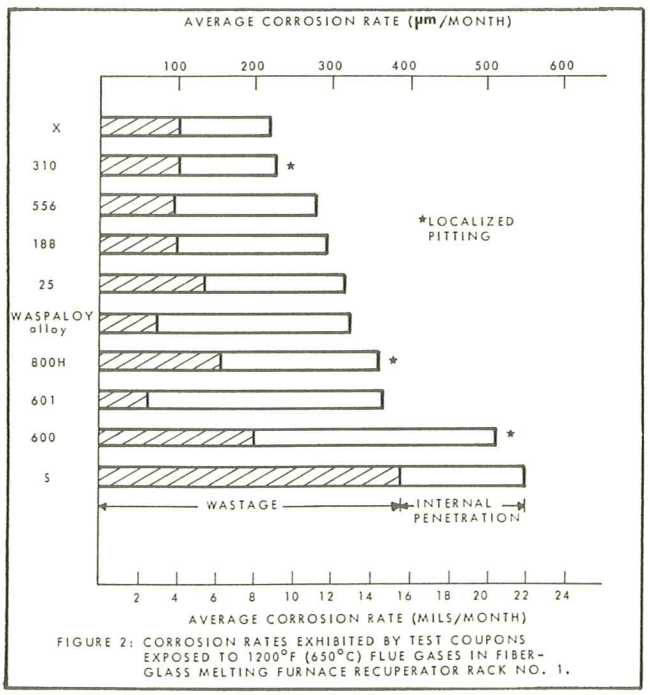

FIGURE 2: CORROSION RATES EXHIBITED BY TEST COUPONS EXPOSED TO 1200°F (650°C) FLUE GASES IN FIBERGLASS MELTING FURNACE RECUPERATOR RACK NO. 1.

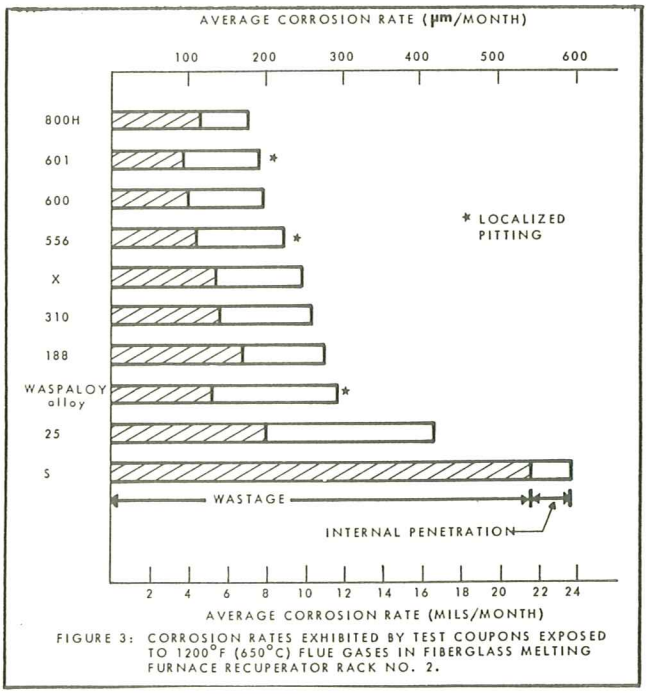

FIGURE 3: CORROSION RATES EXHIBITED BY TEST COUPONS EXPOSED TO 1200°F (650°C) FLUE GASES IN FIBERGLASS MELTING FURNACE RECUPERATOR RACK NO. 2.

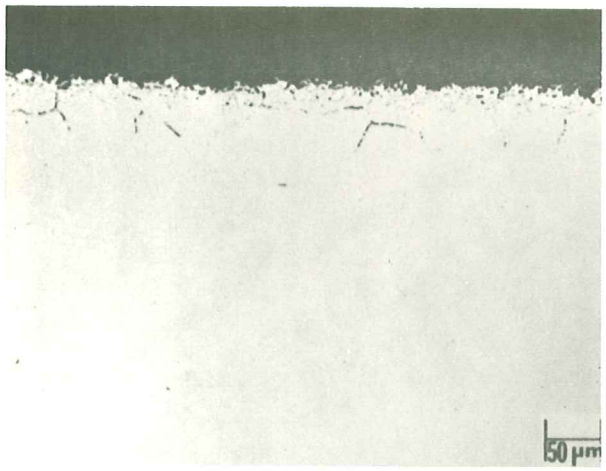

ALLOY X

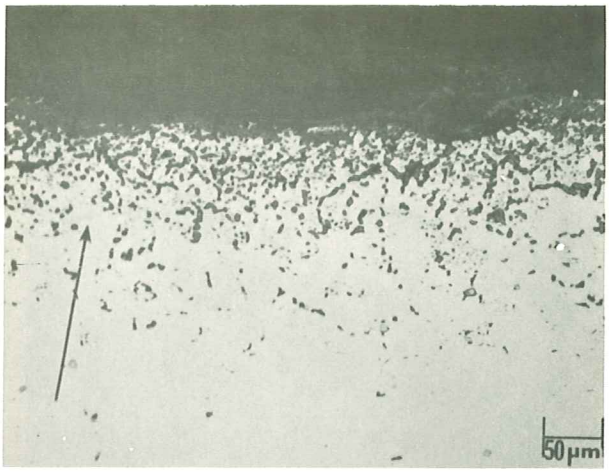

ALLOY 601

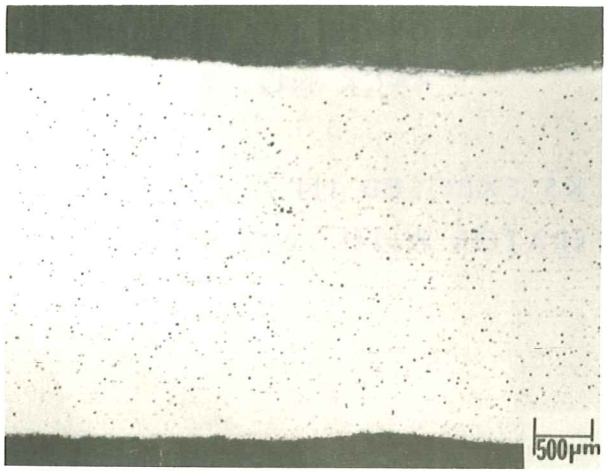

ALLOY X

ALLOY 601

FIGURE 4: MICROSTRUCTURES FOR ALLOY X AND ALLOY 601 COUPONS EXPOSED IN FIBERGLASS MELTING FURNACE RECUPERATOR RACK NO. 1. ARROW IN ALLOY 601 MICROGRAPH INDICATES SULFIDES PRESENT. DARK PARTICLES ARE OXIDES.

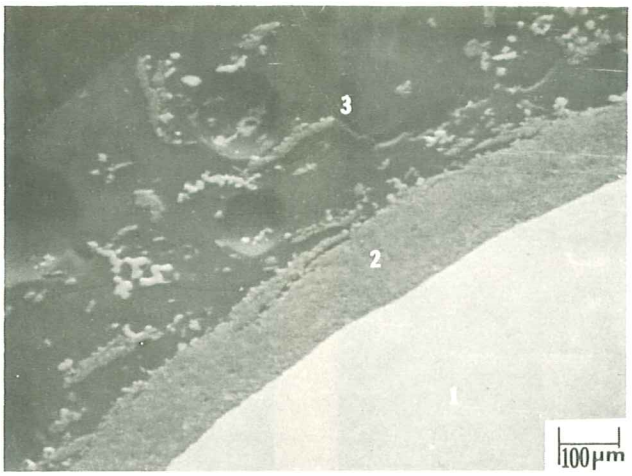

SEMI-QUANTITATIVE ANALYSIS

AREA	Cr	Fe	Co	Ni	W	S	K	Ca
1	35.4	2.6	44.4	6.6	10.8	-	-	-
2	64.5	1.7	19.5	0.8	2.5	1.1	3.4	6.4
3	0.2	0.3	4.4	-	8.2	2.3	25.4	59.0

FIGURE 5: SEM THROUGH-THICKNESS MICROGRAPH OF ALLOY 25 CHAIN USED TO SUPPORT RACK IN FIBERGLASS MELTING FURNACE RECUPERATOR.

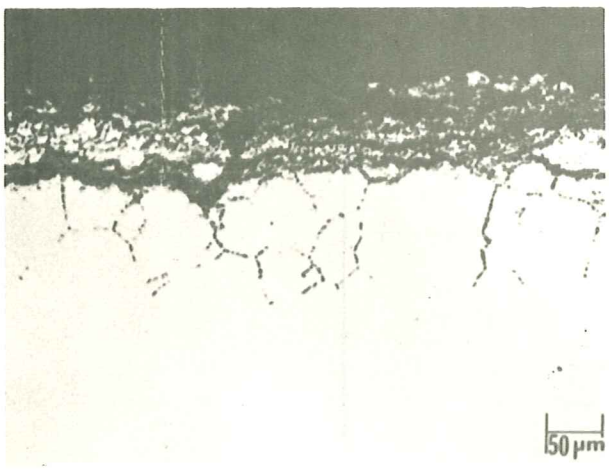

ALLOY X

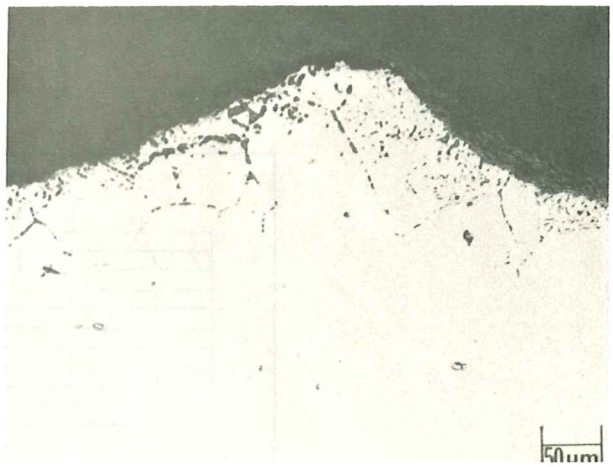

ALLOY 601

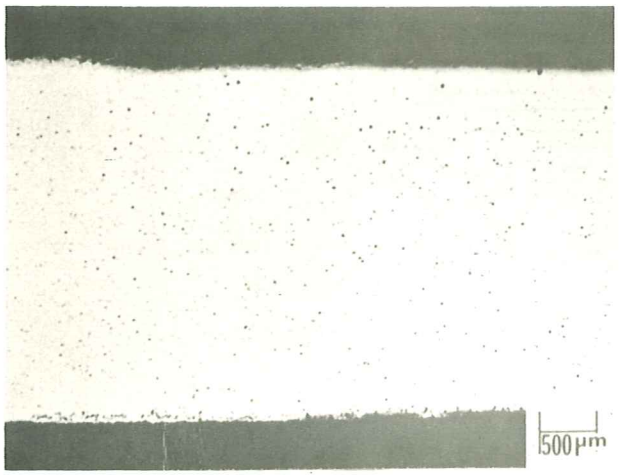

ALLOY X

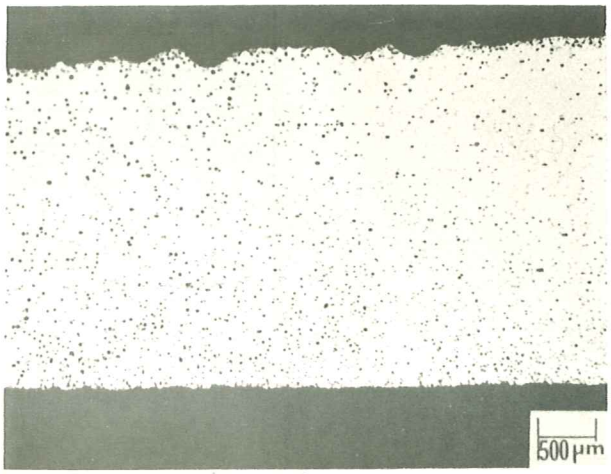

ALLOY 601

FIGURE 6: MICROSTRUCTURES FOR ALLOY X AND ALLOY 601 COUPONS EXPOSED IN FIBERGLASS MELTING FURNACE RECUPERATOR RACK NO. 2.

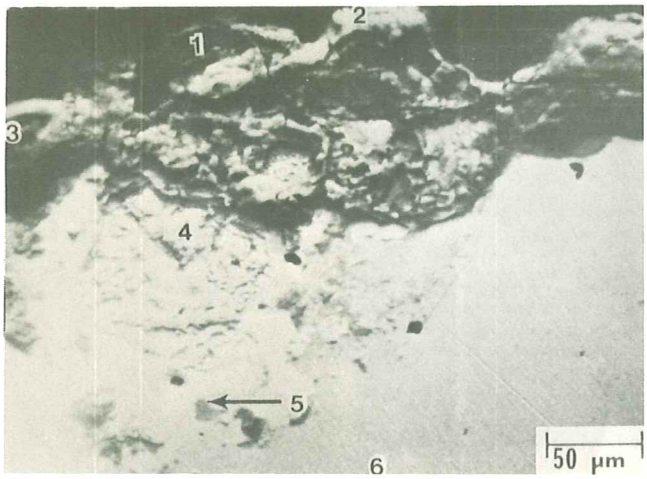

SEMI-QUANTITATIVE ANALYSIS

AREA	Fe	Cr	Si	Al	Ti	Co	K	S	Cl
1	9.5	3.8	32.0	2.4	0.5	47.7	0.9	1.1	2.1
2	75.2	10.3	1.0	-	-	1.7	2.1	1.9	7.8
3	77.6	1.6	1.3	-	-	0.5	3.3	3.6	12.1
4	65.7	32.2	1.7	0.1	-	-	-	-	-
5	67.9	29.2	0.9	0.2	-	-	-	0.4	1.2
6	73.4	25.6	0.8	0.2	-	-	-	-	-

FIGURE 7: SEM THROUGH-THICKNESS MICROGRAPH AND SELECTED AREA EDAX SEMI-QUANTITATIVE ANALYSES FOR FAILED 12 Cr FERRITIC STAINLESS RECUPERATOR TUBE FROM A REVERBERATORY ALUMINUM SCRAP MELTING FURNACE.

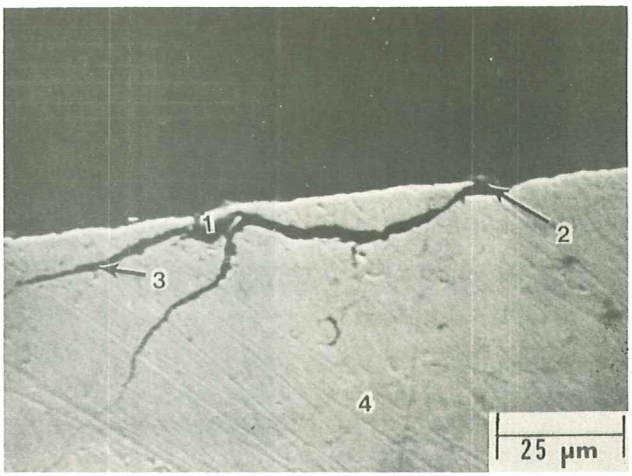

SEMI-QUANTITATIVE ANALYSIS

AREA	Fe	Cr	Si	Al	Ti	Co	K	S	Cl	Br
1	70.6	12.7	0.6	-	0.2	0.8	-	1.1	11.2	2.7
2	73.9	16.3	2.2	1.1	1.7	1.1	1.7	1.3	0.5	-
3	39.1	56.8	0.5	0.7	0.6	0.7	0.5	0.6	0.4	-
4	72.5	26.0	1.2	0.2	-	-	-	-	-	-

FIGURE 8: SEM THROUGH-THICKNESS MICROGRAPH AND SELECTED AREA EDAX SEMI-QUANTITATIVE ANALYSES FOR FAILED 12 Cr FERRITIC STAINLESS RECUPERATOR TUBE FROM A REVERBERATORY ALUMINUM SCRAP MELTING FURNACE.

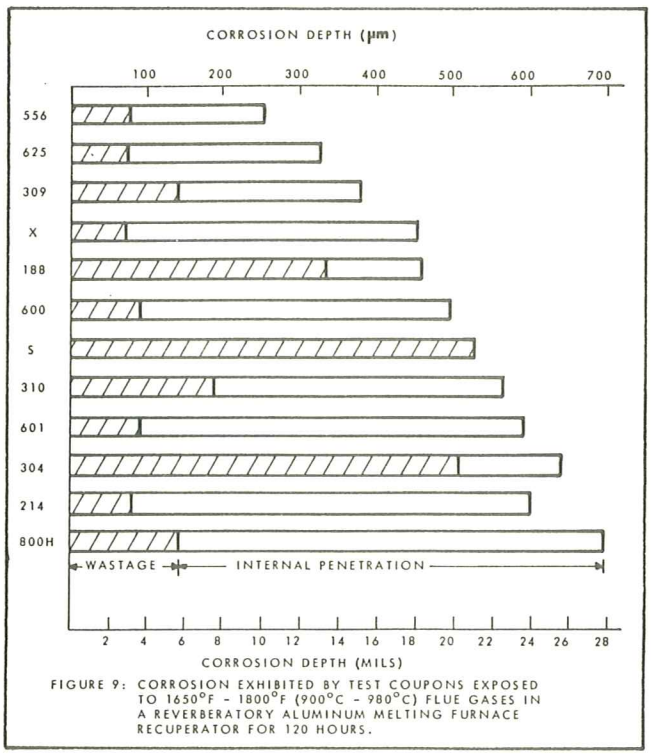

FIGURE 9: CORROSION EXHIBITED BY TEST COUPONS EXPOSED TO 1650°F - 1800°F (900°C - 980°C) FLUE GASES IN A REVERBERATORY ALUMINUM MELTING FURNACE RECUPERATOR FOR 120 HOURS.

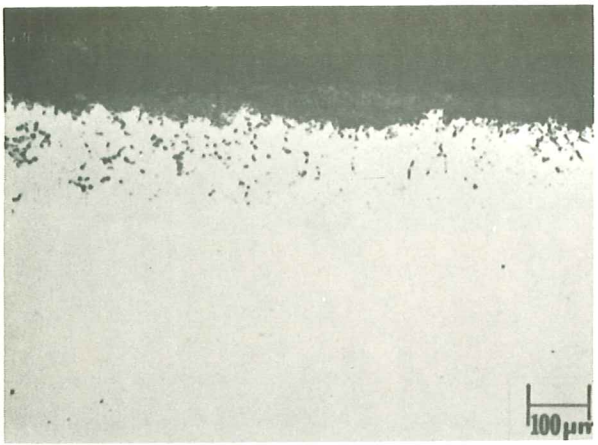

ALLOY 556

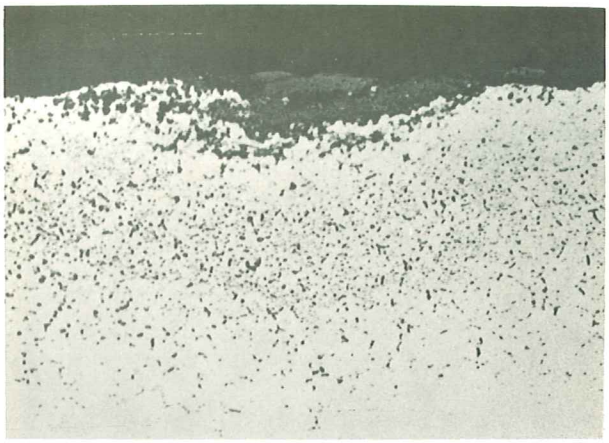

ALLOY 601

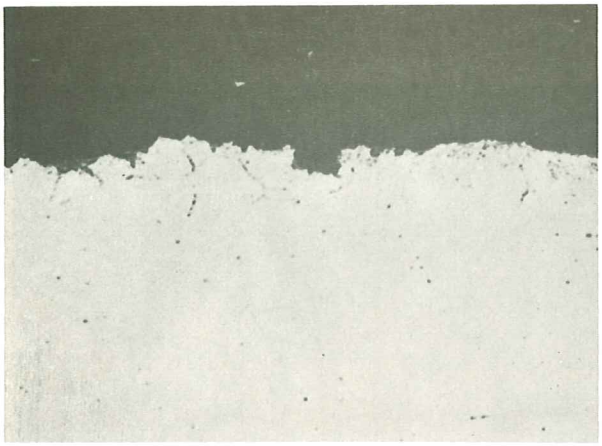

ALLOY 188

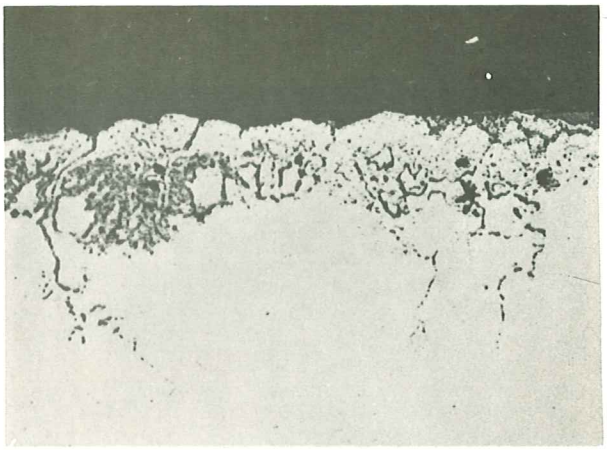

310 STAINLESS

FIGURE 10: MICROSTRUCTURES OF VARIOUS ALLOY COUPONS EXPOSED IN THE REVERBERATORY ALUMINUM MELTING FURNACE RECUPERATOR.

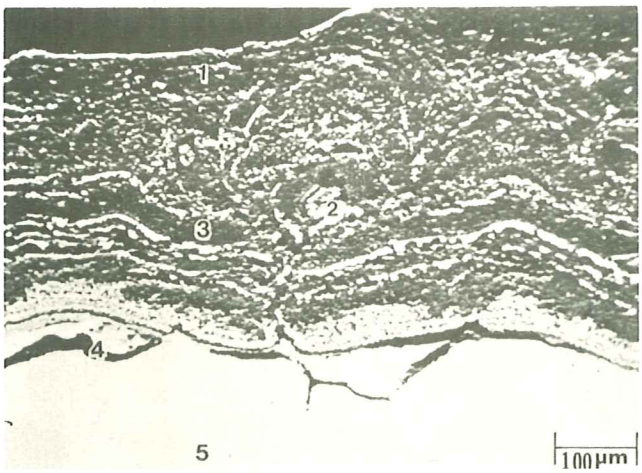

SEMI-QUANTITATIVE ANALYSIS

AREA	Fe	Ni	Cr	Si	S	Co
1	54.4	2.0	41.4	1.3	-	0.9
2	51.9	38.4	9.5	-	-	-
3	60.6	0.5	38.8	-	-	-
4	36.2	3.5	36.2	2.0	21.9	-
5	66.9	5.6	26.6	0.7	-	-

FIGURE 11: SEM THROUGH-THICKNESS MICROGRAPH AND SELECTED AREA EDAX SEMI-QUANTITATIVE ANALYSIS FOR 304 STAINLESS STEEL COUPON EXPOSED IN THE REVERBERATORY ALUMINUM MELTING FURNACE RECUPERATOR.

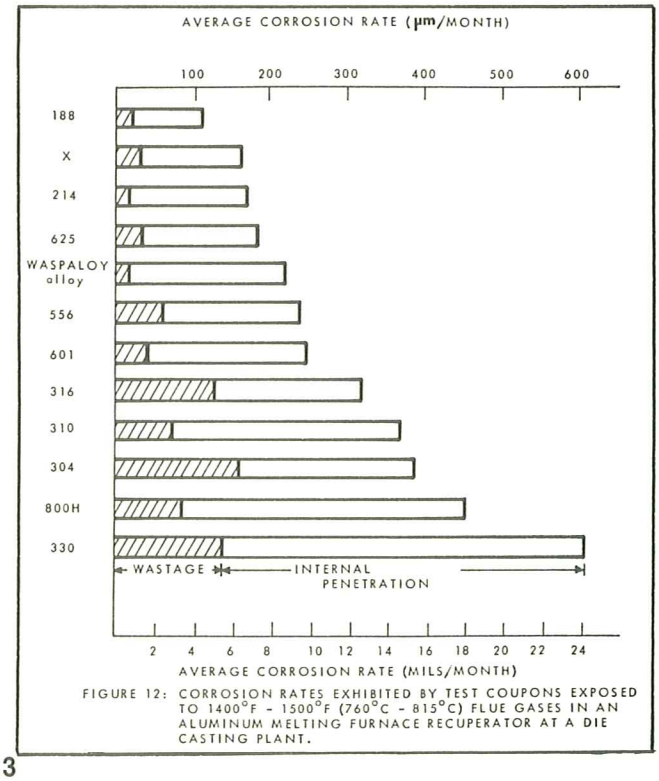

FIGURE 12: CORROSION RATES EXHIBITED BY TEST COUPONS EXPOSED TO 1400°F - 1500°F (760°C - 815°C) FLUE GASES IN AN ALUMINUM MELTING FURNACE RECUPERATOR AT A DIE CASTING PLANT.

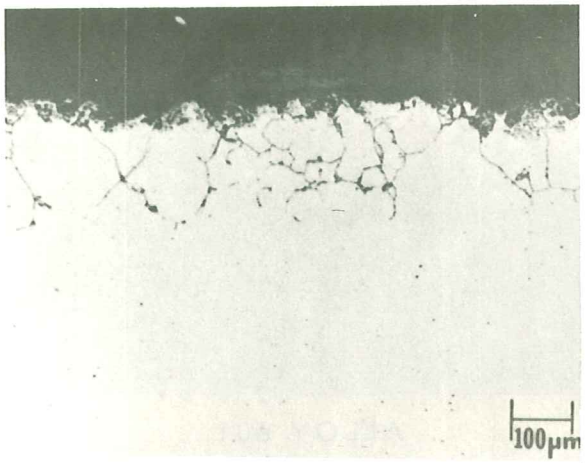

ALLOY 188

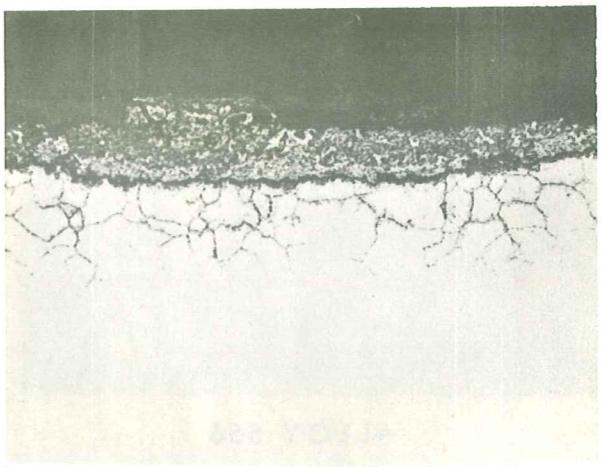

ALLOY X

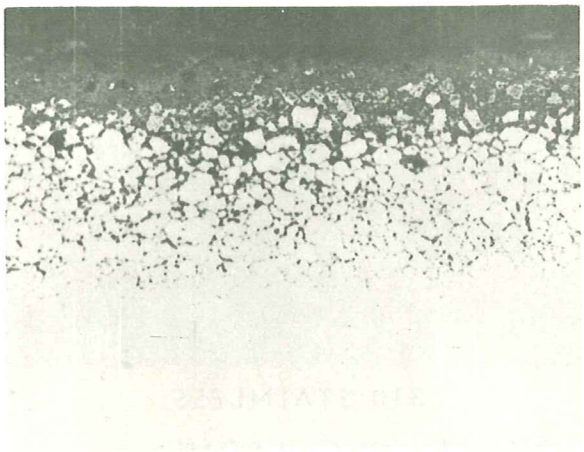

316 STAINLESS

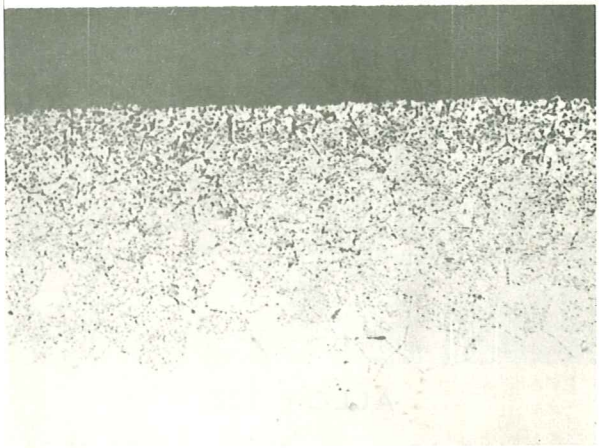

ALLOY 601

FIGURE 13: MICROSTRUCTURES OF VARIOUS ALLOY COUPONS EXPOSED IN THE ALUMINUM MELTING FURNACE RECUPERATOR AT THE DIE CASTING PLANT.

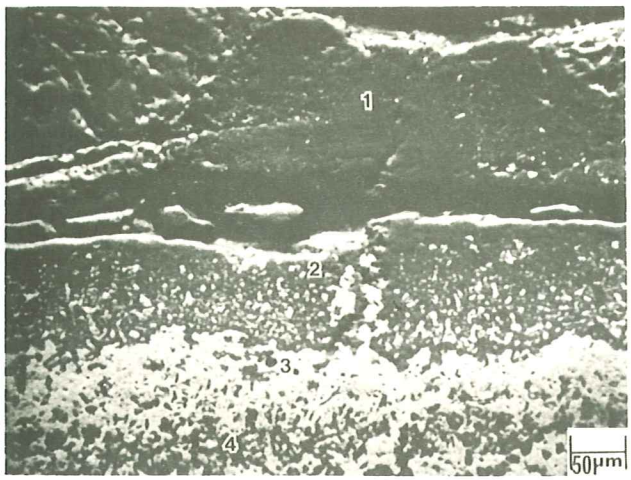

SEMI-QUANTITATIVE ANALYSIS

AREA	Fe	Ni	Cr	Ti	Si	S	Cl
1	1.8	0.3	97.1	0.7	-	-	-
2	1.6	1.0	95.7	0.1	1.5	0.1	-
3	61.6	29.3	8.1	-	0.5	0.2	-
4	13.8	5.4	72.1	0.1	5.6	0.2	2.8

FIGURE 14: SEM THROUGH-THICKNESS MICROGRAPH AND SELECTED AREA EDAX SEMI-QUANTITATIVE ANALYSES FOR 310 STAINLESS STEEL COUPON EXPOSED IN THE ALUMINUM DIE CASTING PLANT MELTING FURNACE RECUPERATOR.

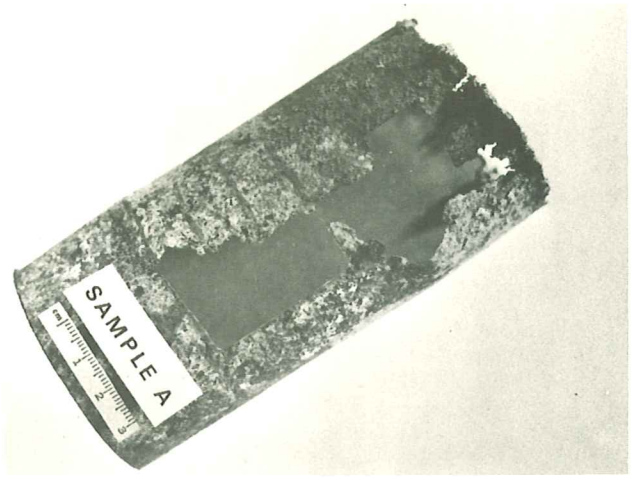

FIGURE 15: PERFORATED 316 STAINLESS TUBE FROM THE FIRST ROW OF A RECUPERATOR IN A ZINC MELTING FURNACE. TUBE FAILED AFTER 2 OR 3 MONTHS EXPOSURE TO 1800°F (980°C) FLUE GASES.

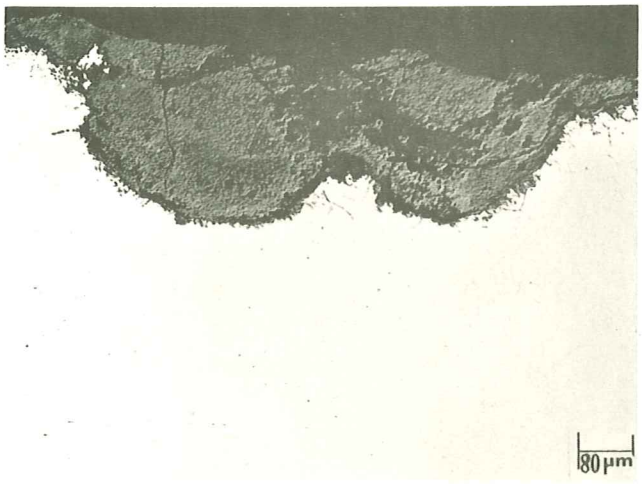

FIGURE 16: THROUGH-THICKNESS MICROSTRUCTURE OF 316 STAINLESS RECUPERATOR TUBE WHICH FAILED IN ZINC MELTING FURNACE APPLICATION. SIDE FACING FLUE GAS FLOW IN THE FIRST ROW OF TUBES.

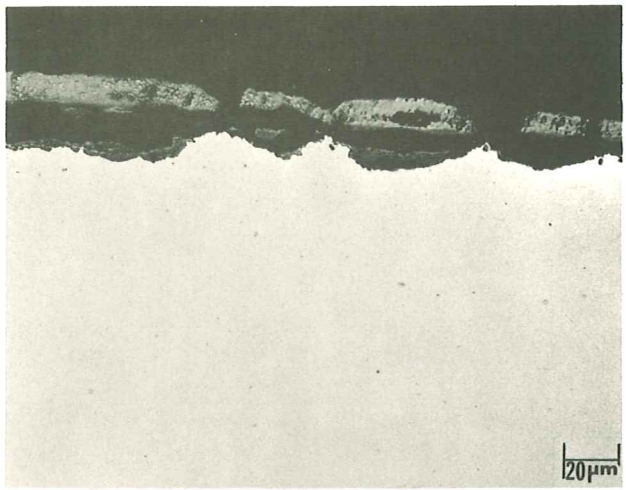

FIGURE 17: THROUGH-THICKNESS MICROSTRUCTURE OF 316 STAINLESS RECUPERATOR TUBE WHICH FAILED IN ZINC MELTING FURNACE APPLICATION. SIDE FACING FLUE GAS FLOW IN THE THIRD ROW OF TUBES.

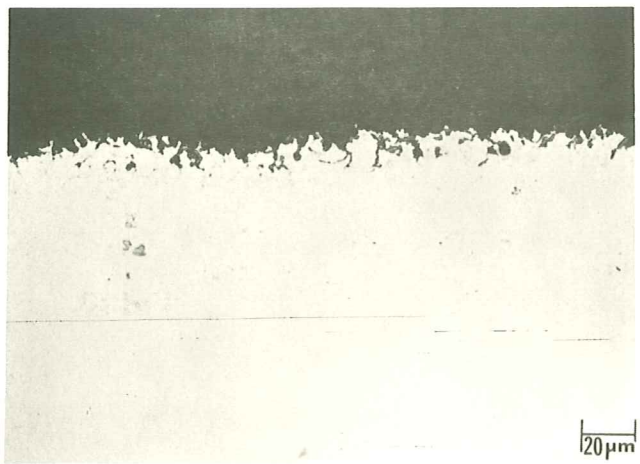

FIGURE 18: THROUGH-THICKNESS MICROGRAPH OF 309 STAINLESS BAFFLE PLATE FROM ZINC MELTING FURNACE RECUPERATOR.